Dust Accumulation and Lifting at the Landing Site of the Mars 2020 Mission, Jezero Crater, as Observed From MEDA

A. Vicente-Retortillo, M. T. Lemmon, G. M. Martinez, D. Toledo, V. Apéstigue, I. Arruego, T. Bertrand, R. Lorenz, E. Sebastián, R. Hueso, et al.

Geophysical Research Letters

RESEARCH LETTER
10.1029/2023GL107975

Dust Accumulation and Lifting at the Landing Site of the Mars 2020 Mission, Jezero Crater, as Observed From MEDA

A. Vicente-Retortillo[1], M. T. Lemmon[2], G. M. Martinez[3], D. Toledo[4], V. Apéstigue[4], I. Arruego[4], T. Bertrand[5], R. Lorenz[6], E. Sebastián[1], R. Hueso[7], C. Newman[8], M. D. Smith[9], and J. A. Rodriguez-Manfredi[1]

[1]Centro de Astrobiología (CAB), CSIC-INTA, Torrejón de Ardoz, Spain, [2]Space Science Institute, Boulder, CO, USA, [3]Lunar and Planetary Institute, Universities Space Research Association, Houston, TX, USA, [4]Instituto Nacional de Técnica Aeroespacial (INTA), Torrejón de Ardoz, Spain, [5]LESIA, Paris Observatory, Meudon, France, [6]JHU/APL, Laurel, MD, USA, [7]Universidad del País Vasco UPV/EHU, Bilbao, Spain, [8]Aeolis Research, Chandler, AZ, USA, [9]NASA Goddard Space Flight Center, Greenbelt, MD, USA

Abstract We quantify the effect of dust accumulation at Jezero crater by means of a Dust Correction Factor (DCF) for the solar radiation measured by the photodiodes of the Radiation and Dust Sensor of the Mars 2020 mission. After one Mars Year, dust on the photodiode surface attenuated 25%–30% of the incoming solar radiation. The DCF did not decrease monotonically; we use a model to reproduce its evolution and to derive dust deposition and lifting rates, showing that dust removal is 9 times larger at Jezero crater than at InSight's location in western Elysium Planitia. The model fit obtained using observed opacities is further improved when fed with dust sedimentation rates simulated by a GCM that considers a particle size distrtibution. Projections show seasonal net dust removal, being encouraging for the long-term survival of solar-powered missions to Jezero or similarly active dust lifting regions.

Plain Language Summary Dust is ubiquitous in the Martian atmosphere, accumulating on both natural and artificial surfaces. Dust particularly affects the performance and lifetime of missions: the termination of InSight and MER-B operations are recent examples. Dust accumulation shows a seasonal behavior, and attenuated 25%–30% of the incoming solar radiation on Perseverance after the first Mars Year of the mission. Dust removal is almost 10 times larger than at InSight's location: projections indicate that surfaces at Jezero will be periodically partially cleaned. The estimations of the effect of the accumulated dust as a function of time are encouraging for solar-powered missions to regions with similar amounts of dust lifting, which might be determined from orbital data on where dust storms originate, dust devils or their tracks are found, or seasonal albedo changes are noted. In addition, the quantification of the effect of accumulated enables future studies requiring more accurate knowledge of incoming solar radiation at the surface.

Key Points:

- We present the evolution of dust accumulation at Jezero crater for more than one Mars Year
- We derive dust deposition and removal rates: removal is 9 times more efficient than at the InSight location in western Elysium Planitia
- Projections show that surfaces at Jezero will experience seasonal net dust removal, encouraging solar-powered missions

Supporting Information:

Supporting Information may be found in the online version of this article.

Correspondence to:

A. Vicente-Retortillo,
adevicente@cab.inta-csic.es

Citation:

Vicente-Retortillo, A., Lemmon, M. T., Martinez, G. M., Toledo, D., Apéstigue, V., Arruego, I., et al. (2024). Dust accumulation and lifting at the landing site of the Mars 2020 mission, Jezero crater, as observed from MEDA. *Geophysical Research Letters*, *51*, e2023GL107975. https://doi.org/10.1029/2023GL107975

Received 12 JAN 2024
Accepted 4 APR 2024

1. Introduction

Dust is present in the Martian atmosphere throughout the year, posing challenges to the exploration of the planet, especially for solar-powered missions. Dust accumulation on solar panels gradually reduces the amount of energy they can generate, while large atmospheric dust opacities during global dust storms greatly reduce the solar radiation reaching the surface for weeks or longer. The recent termination of InSight and Mars Exploration Rover (MER) B operations indicate that understanding the role of dust accumulation in attenuating solar radiation is vital for solar-powered missions. Quantification of dust accumulation and its evolution is thus critical for future Mars missions, as solar power is the most practical solution for reduced-cost missions (MEPAG MCE-SAG, 2023). In addition, the combined analysis of the temporal evolution of dust accumulation and contemporaneous environmental variables provides insight into dust lifting processes and dust deposition and removal rates, as is called for by both the latest MEPAG Goals document (Goal II, A2.1; MEPAG, 2020) and Planetary Science and Astrobiology Decadal Survey (Strategic Research for Q6.4, NASEM, 2022).

The results presented here are also vital to enhancing the scientific return of Mars 2020 because solar radiation measurements available in the Planetary Data System (PDS) are not corrected for the effect of dust accumulation on the sensor. As just one example, our results allow reassessments and new calculations of key geophysical

properties of the terrain through the rover traverse (e.g., albedo and thermal inertia; Martínez et al., 2023), helping to interpret the geological and environmental context of the terrain experienced by Perseverance.

Dust accumulation has been typically studied from the analysis of solar panel currents, first from Pathfinder (Crisp et al., 2004; Rover Team, 1997) and then from MER, which provided the first long-term temporal series (Stella & Herman, 2010). Unfortunately, the MERs did not include meteorological sensors that could measure the conditions required for dust removal events. The Mars Science Laboratory (MSL) mission helped filling this gap: Rover Environmental Monitoring Station (REMS) measurements in combination with mesoscale simulations enabled the evolution of dust accumulation to be linked to dust removal processes (Vicente-Retortillo et al., 2018). A summary of the different behavior in net dust accumulation between missions prior to Mars 2020 can be found in Lorenz et al. (2021). More recently, Vicente-Retortillo et al. (2023) assessed the processes affecting dust lifting at Jezero crater by analyzing sudden changes in surface albedo caused by dust devils passing over the Perseverance rover. However, the frequent motion of the rover does not allow the long-term study of dust accumulation on natural surfaces.

Since February 2021, the Mars Environmental Dynamics Analyzer (MEDA; Rodríguez-Manfredi et al., 2021), onboard the Mars 2020 Perseverance rover at Jezero crater, has been monitoring changes in atmospheric variables such as solar radiation, pressure and wind, which are complemented by Mastcam-Z observations of atmospheric opacity (Lemmon et al., 2022; Martínez et al., 2023). As described in this paper, such measurements allow both the analysis of the temporal evolution of dust accumulation and insight into its causes.

Quantification and future predictions of dust accumulation are important for not only future solar-powered Mars missions, but also to estimate the likely dust accumulation on sample tubes deposited on the surface, which will be exposed to dust accumulation for years (Farley et al., 2020).

2. Materials and Methods

2.1. Instruments, Observations, and Data Used in This Work

The quantification of dust accumulation at Jezero crater relies on solar fluxes measured by MEDA and dust opacities derived from Mastcam-Z observations, which are/are not impacted by dust accumulation, respectively. MEDA includes a Radiation and Dust Sensor (RDS; Apéstigue et al., 2022) and a sky-facing camera named Skycam (Rodríguez-Manfredi et al., 2021), both located on the rover deck. The RDS consists of two sets of eight photodetectors, with one set pointing at the zenith in several bands between ultraviolet and near infrared wavelengths, and the other set pointing sideways, mostly at an elevation of 20°. In this work, we use measurements from the upward-looking TOP7 channel (190–1,200 nm), which is the only channel with a hemispheric field of view. RDS measurements are acquired at 1 Hz during at least the first 5 min of each hour, with extended sessions that vary in time of day and duration but typically cover every other hour. The RDS photodetectors are distributed around Skycam, which provides 124° views of the sky and allows direct solar flux measurements when the Sun is within a region obscured by an annular neutral density (ND) coating (Rodríguez-Manfredi et al., 2021). Mastcam-Z is a multispectral stereo pair of CCD cameras (Bell et al., 2021) that allows the determination of dust opacity from Sun imaging using solar filters (Lemmon et al., 2015, 2024). For the InSight mission, we use the results of dust accumulation obtained in Lorenz et al. (2021), which were derived from the solar array currents and suspended dust optical depth (Lorenz et al., 2020).

2.2. Methodology to Retrieve the Dust Correction Factor

The methodology employed in this work relies heavily on that developed for the MSL REMS UV measurements (Vicente-Retortillo et al., 2018, 2020). We quantify the effect of accumulated dust by means of the Dust Correction Factor (DCF), which indicates the fraction of the incoming radiation at the surface that reaches the photodiode through the dust accumulated on the window. Unlike for REMS, where the relative variation in the DCF was calculated by comparing measurements under similar Sun positions on different sols, the pre-flight characterization of the angular response of the RDS detector allows the retrieval of the absolute value of the DCF for any sol, greatly simplifying its calculation. We describe below the steps of the updated methodology.

First, we use the radiative transfer model COMIMART (Vicente-Retortillo et al., 2015) and the rover tilt and orientation to simulate hourly values of the surface solar flux (F) between 190 and 1,200 nm. COMIMART is fed with Mastcam-Z opacities and includes dust radiative properties obtained from the refractive indices derived by

Wolff et al. (2009, 2010). We also use COMIMART and the TOP7 angular response function to convert TOP7 measurements to total fluxes by means of a conversion factor (C) that depends on solar zenith angle and atmospheric opacity. For each sol, we calculate hourly values corresponding to the first 5 min of measurements of each hour, and select the highest value (M) after discarding those affected by sharp variations produced by rover activities or dust devils. Finally, the effect of accumulated dust is DCF = $M{\cdot}C/F$.

We follow a similar approach for Skycam observations, but now the DCF is obtained from synthetic aperture photometry of the imaged solar flux. As discussed in Section 3.1, we now rely on the attenuation of the direct solar flux instead of on the total flux, so values derived from the TOP7 measurements are more closely related to solar panels than those from Skycam.

2.3. Retrieval of Dust Deposition and Removal Rates

Dust deposition and removal rates are obtained by using a simple physical model for the DCF and finding its corresponding parameters that best fit the observations. The conceptual basis of the model, which relies on previous efforts (Kinch et al., 2007; Yingst et al., 2020), is that dust deposition depends on atmospheric dust opacity and that there is a fractional dust removal per sol. Specifically, the DCF for a given sol relies on the conditions for the previous sol:

$$\mathrm{DCF}_{i+1} = \mathrm{DCF}_i \cdot \exp(-D \cdot \tau_i + R \cdot (1 - \mathrm{DCF}_i)) \quad (1)$$

Here, τ is the dust opacity obtained from Mastcam-Z, and D and R are dimensionless parameters that depend on the efficiency of dust deposition and removal, which can be affected not only by environmental conditions, but also by the surface properties. The first term of the exponential indicates that deposition is expected to increase with the amount of suspended dust above the rover; the second term indicates that the effect in DCF of removing a fraction of the accumulated dust increases with dust cover. When the first/second term dominates, the surface experiences net dust accumulation/removal, respectively. We also use the ratio R/D to discuss the relative efficiency of dust removal mechanisms compared to that of dust deposition at each landing site (a low value indicates inefficient dust removal mechanisms). We perform Monte Carlo simulations for 10^5 combinations of D and R. Due to the nature of the model, there is a degeneracy in the solutions (Section 3.1). For this reason, we select the simulations with a RMSE below 110% of that of the best fit (for completeness, we depict those below 125%), and among them we select the 5th, 50th and 95th percentiles of D and R for each site, physically representing scenarios of low, average and high efficiency of deposition and removal processes, respectively.

3. Results

3.1. Temporal Evolution of Dust Accumulation

Figure 1 shows DCF values obtained from the RDS TOP7 measurements during the first 777 sols of the Mars 2020 mission (red). The thick black line shows the smoothed temporal evolution, the dashed lines show the corresponding limits considering the standard deviation of the DCF using 40-sol windows, and the gray markers indicate the 880 nm opacities measured with Mastcam-Z.

On the first sols of the mission, the value of the DCF was around 0.92, indicating that the incoming solar radiation was already attenuated. This value is consistent with independent estimations of dust accumulation on the upward-looking channels of the MEDA Thermal Infrared Sensor (TIRS; Martínez et al., 2023; Sebastián et al., 2020), which showed a degradation of ∼9% during the first sols. This behavior was likely caused by the deposition of dust lifted during landing, as supported by an image acquired on sol 84 showing small amounts of dust accumulation (Figure 1, bottom).

During the MY 36 northern spring and summer seasons ($L_s < 180°$, sols 1–361), dust accumulation increased at a very slow but relatively constant rate. The image of the RDS on sol 324 shows an increase in dust accumulation. The MY 37 northern spring (after sol 658) is also characterized by a virtual lack of net dust accumulation.

The DCF experienced a strong decrease during the dustier northern fall and winter seasons ($L_s > 180°$, sols 362–657), when the opacity was above 1 during sols 415–475 and 570–610, which correspond to the annually occurring A and C large regional dust storm activity periods (Kass et al., 2016; Martín-Rubio et al., 2024). Although on short time-scales there might be periods of no correlation between net dust accumulation and

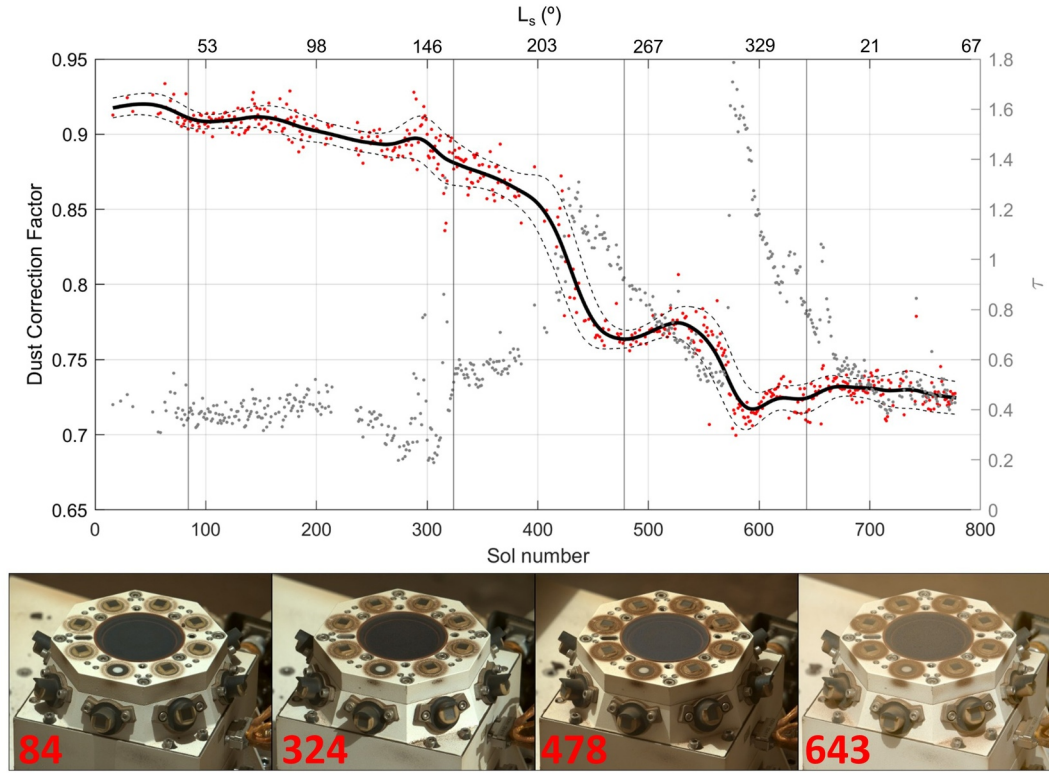

Figure 1. (top) Temporal evolution of the Dust Correction Factor during the first 777 sols of the Mars 2020 mission. Individual observations and a smoothed fit are represented with red dots and a black thick line. The dashed lines represent the uncertainty, obtained from the standard deviation of the individual observations over 40-sol windows. Gray dots represent atmospheric opacity (τ). Vertical lines indicate the sols of the images shown in the bottom panel. (bottom) Mastcam-Z images of the Radiation and Dust Sensor (RDS) on four representative sols, indicated in red. Skycam is visible in the center of the RDS, surrounded by the two sets of photodiodes (the upward-looking set is the innermost one).

atmospheric opacity, a global analysis indicates that most of the net dust accumulation occurred around these two periods of enhanced atmospheric dust content. Images corroborate the increase in dust accumulation between sols 324 and 478; the visual comparison between sols 478 and 643 remains inconclusive, partly due to changes in illumination (Figure 1, bottom).

While current limitations in the quality and illumination of Mastcam-Z images of the RDS preclude accurate estimations of DCF, they can be used to provide a broader context, including spatial differences in dust accumulation. Figure 1 shows that the pattern of the accumulated dust is clearly driven by the magnets that surround each photodiode. This raised the question of whether the dust accumulation evolution on the photodiode could be extrapolated to other surfaces not affected by magnets. Figure S1 in Supporting Information S1 compares the evolution of dust accumulation on the RDS TOP7 channel window (red) to that on the Skycam window (blue), which is not affected by magnets. There are three differences between both series. First, the noise of Skycam values is significantly larger (noise sources are discussed in Supporting Information S1). This highlights the importance of photodiode measurements in quantifying the effect of dust accumulation with small uncertainties. Skycam DCF is derived from solar images, and therefore it represents the effect of dust on approximately 0.04% of the window, which varies for each image (the relative Sun position depends on time and rover orientation). Considering the total radiation instead of the direct one would require estimating the diffuse radiation obscured by the ND coating, which strongly depends on the aerosol phase function and hence on aerosol properties (Vicente-Retortillo et al., 2017), and would add sources of uncertainty. Second, the Skycam window appears to have been affected by a relatively strong dust removal event during the L_s 155 small regional dust storm (passing over Jezero around sol 315), which is not observed on the TOP7 channel, and could be related to encounters with strong vortices during the dust storm (Hueso et al., 2023; Lemmon et al., 2022). Third, Skycam shows a larger net dust accumulation rate between sols 400 and 600. Besides these differences, dust accumulation on both surfaces shows

a very similar temporal evolution, with a relatively constant value during the first 300 sols and after sol 600, and with dust accumulation occurring mainly between sols 400 and 600. In summary, it appears that magnets mitigate the effect of dust deposition, but also that they reduce the mobility of deposited dust, hindering dust removal events. Due to the global similarities between both series, we will focus on the values obtained from the RDS TOP7 channel due to their significantly smaller uncertainties.

3.2. Dust Lifting and Deposition Rates: A Quantitative Comparison Between Perseverance and InSight Locations

After one MY, accumulated dust attenuates between 25% and 30% of the incoming solar radiation. This value is significantly smaller than for previous missions such as InSight. Lorenz et al. (2021) showed that, in the absence of dust removal, the DCF typically decreases by 0.2% per sol. Following this rate, the DCF after 1 year should be $DCF_1 \sim 0.998^{669}$–0.26. This difference indicates that there is a persistent dust removal mechanism at Jezero crater that significantly mitigates the effect of dust accumulation (it could also indicate extraordinarily low dust deposition rates but this is unlikely, since annual average dust sedimentation rates (DSRs) are fairly uniform across landing sites (Lorenz et al., 2021)). Compared to other missions, the small net accumulation during the first 300 sols could be explained by the low atmospheric opacity and the frequent dust lifting events at Jezero crater during this period (Hueso et al., 2023; Lemmon et al., 2022; Newman et al., 2022; Toledo et al., 2023; Vicente-Retortillo et al., 2023). In this section, we use results of the simple physical model to derive dust lifting and deposition rates from DCF measurements, and we perform comparisons between Jezero crater and InSight's location in western Elysium Planitia.

Figure 2 shows a comparison of the model parameters that best fit the observations at the locations of the Perseverance rover and the InSight lander. The top panel shows the combinations of D and R with a RMSE not exceeding 125% of that of the best fit. It illustrates the clear differences between both locations: dust removal efficiency is one order of magnitude larger at Jezero. Specifically, the median of the values of R that provide a good fit for Jezero is 9.2 times its counterpart for InSight ($49.5 \cdot 10^{-4}$ vs. $5.4 \cdot 10^{-4}$).

The smaller differences in D (median values of $18.8 \cdot 10^{-4}$–$26.6 \cdot 10^{-4}$ for Jezero and InSight) could be partially attributed to the different features of the InSight solar arrays and the MEDA TOP7 detector. The main potential cause is that dust deposition on the TOP7 detector could be mitigated due to the surrounding magnet, which would be consistent with the lower value of D. Another possibility is that the effective DCF for a given amount of dust may be slightly affected by the different spectral responses of the arrays and the detector (similar to the wavelength dependence of atmospheric opacity); however, the response of the arrays is more similar to that of the TOP7 photodiode than to that of the MSL REMS photodiodes (Apéstigue et al., 2022; Crisp et al., 2004; Vicente-Retortillo et al., 2020), and Lorenz et al. (2021) showed that REMS DCF growth due to deposition was not qualitatively different from that for InSight.

The middle and bottom panels show the observed DCF for Jezero crater and western Elysium Planitia, respectively, together with three model runs that fit well to those observations. These simulations correspond to the 5th, 50th and 95th percentile of the combinations of D and R that provide a RMSE below 110% of the best fit (values are shown in the legend); physically, these simulations correspond to scenarios in which deposition and lifting processes have low, average and high efficiency, respectively.

In the case of western Elysium Planitia, we also provide the evolution of the DCF obtained from a decay of 0.2%/sol (thick blue line). This value represents the typical rate in absence of removal (Lorenz et al., 2021). For a mean opacity of 0.8, this rate would correspond to $D \sim 2.4 \cdot 10^{-3}$, in excellent agreement with the center of the ellipse on the top panel, and running the model without the removal term increases the RMSE only by 7%, consistent with the interpretation that, despite the vast number of vortex encounters (Spiga et al., 2021), almost no dust-removing events occurred during the InSight mission. The RMSE from the constant decay is 70% larger than that using the model, supporting the recommendation of using a physical model to predict the DCF. In the case of Jezero crater, only the physical model is able to reproduce the observed behavior due to the high importance of the removal processes.

These results, complemented by those presented in Lorenz et al. (2021), indicate that the efficiency of the removal processes is the dominant variable in the model; hence, the DCF evolution will be more difficult to predict for locations for which dust removal processes have not been measured in situ. However, the model

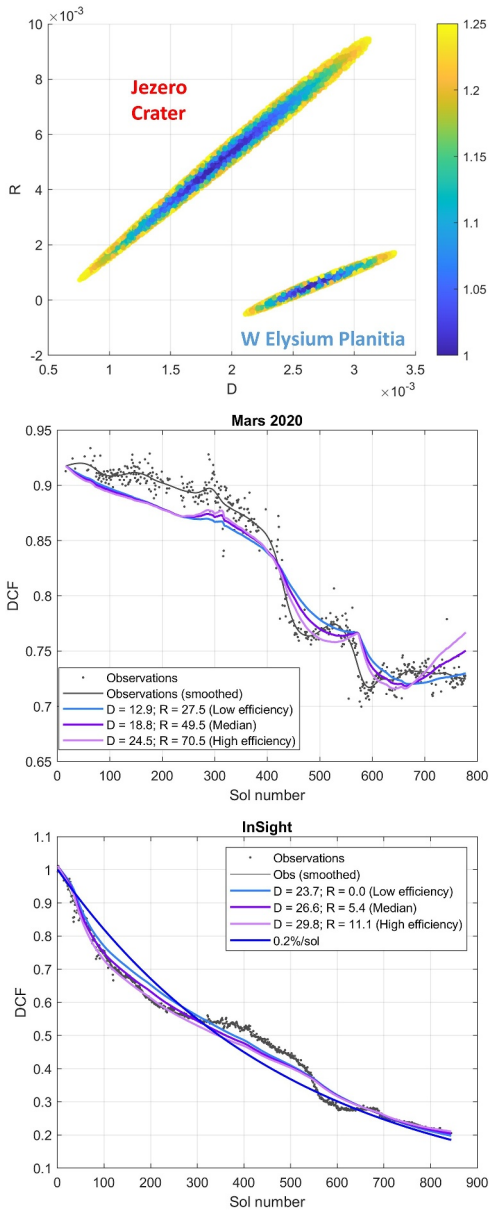

Figure 2. (top) Combinations of dust deposition and removal efficiencies introduced in Equation 1 that best fit the observations. Colors represent the ratio between the RMSE of each combination and the one providing the best fit for each mission. Combinations with $R < 0$ are included to show that the best combinations for InSight occur for R close to 0. (middle) Dust Correction Factor derived from Mars 2020 observations (gray) and model simulations assuming low, average and high efficiency of deposition and removal processes. (bottom) As above, but for InSight, and including a 0.2% decay/sol. D and R values in legends for the middle and bottom panels should be multiplied by 10^{-4}.

parameters obtained from MEDA observations allow projections of the DCF at Jezero crater, as discussed in the following section.

3.3. DCF Simulations From GCM Dust Sedimentation Rates: Assessment and Projections

The dust deposition and removal rates derived above can shed light on power predictions for long-term, solar-powered missions at these locations. Assuming that every year presents the same dust opacity behavior as the first one (a reasonable assumption for years with no global dust storms; Martínez et al., 2017), predictions for both locations clearly differ. In the case of InSight, the effect of dust deposition dominates that of dust removal mechanisms, as quantitatively corroborated by the extremely low dust removal relative efficiency ($R/D \sim 0.2$). The three model runs suggest that dust accumulation would keep increasing with time. Golombek et al. (2023) showed that InSight's DCF after 2 MY was 0.13; our retrieved values of R and D predict that 0.13 would be reached after between 1.6 and 1.8 MY, in good agreement with the observation; part of the difference could be attributed to the lower opacities, hence, reduced dust fallout, during the second local winter (Golombek et al., 2023). Thus, model predictions appear to provide good estimates of long-term dust accumulation, although inaccuracies may arise if interannual variability in opacity is high.

The behavior at Jezero is noticeably different, and none of the three simulations predict a continuous decrease of the DCF due to the significantly larger dust removal relative efficiency ($R/D \sim 2.6$). In contrast, these runs predict that the DCF would enter into an annual cycle. The dust deposition term of Equation 1 depends only on opacity. To test the hypothesis that considering the particle size distribution of suspended dust could further improve the prediction capabilities of our model, we replace in Equation 1 observed opacities with DSRs simulated with the LMD Mars Planetary Climate Model, which accounts for multisize particle sedimentation and simulates the period of the observations by driving the model with orbital dust column opacity maps (details provided in Text S1 of Supporting Information S1).

The top panel of Figure 3 compares the measured opacities at Jezero crater with the GCM simulations of the daily DSRs. In general, there is a good agreement between both variables. However, there are noticeable differences during the second period of enhanced opacity (sols 570–610), when DSRs show a maximum at the beginning of the event and a subsequent abrupt decay. The deposition of the largest (and heaviest) dust particles lofted from the surface at the beginning of the event, unable to be transported elsewhere, is the most likely explanation. These differences provide a unique opportunity to test the performance of both parameters in representing the observed temporal evolution of the DCF.

The middle panel compares the observed DCF (red dots) with the values simulated using opacities (green) and DSRs (blue). During the first 350 sols and from sol 570 onwards, the model relying on DSRs shows excellent performance, virtually matching the observations. The improvement is particularly significant around the second period of enhanced opacity (sols 570–610, see top panel), when the behavior of the DCF could not be accurately captured relying on opacities only. During the first period of enhanced opacities (sols 415–475), both models perform similarly, not fitting well the shape of the observed DCF, but representing accurately the net dust accumulation over this period. This analysis suggests that, although both models provide good estimates of long-term (semiannual, annual or interannual) dust accumulation, DSRs from models guided by observations can more accurately represent the seasonal and shorter-term behavior.

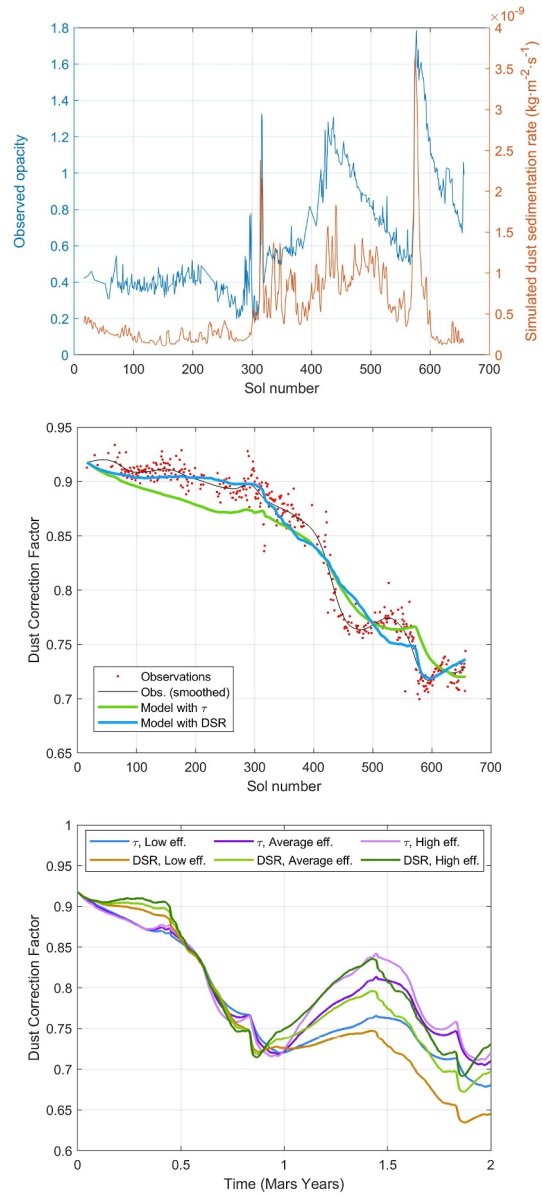

Figure 3. (top) Planetary Climate Model simulations of dust sedimentation rates (DSRs) compared to opacity measurements. (middle) Observed Dust Correction Factor (DCF) (red), and model simulations relying on measured opacity (green) and simulated DSRs from a model guided by orbital opacity maps (blue). (bottom) DCF projections from model runs with different input variables and efficiency parameters.

The bottom panel shows interannual predictions of dust accumulation using opacities and DSRs. The DCF values and annual amplitude depend on the efficiency of the deposition and removal mechanisms: under low efficiency conditions, the projected dust accumulation is larger and the seasonal variability is smaller. Despite these differences, all of the projections indicate that dust accumulation will experience periods of significant net dust removal starting on the second MY.

These projections could be affected by several factors: interannual variability in opacity, sedimentation rates or occurrence of global dust storms; occurrence of strong dust removal events that could lead to a sudden increase in the DCF; and topography-induced variability in the relative efficiency of dust removal mechanisms along the rover traverse. Even considering these caveats, the results presented are encouraging for future missions to Jezero or similarly active dust lifting regions that plan to use solar power as a cost-effective way of operating.

4. Conclusions

We have quantified the effect of dust accumulation at Jezero crater during the first 777 sols of the Mars 2020 mission using measurements by MEDA's RDS. These results are important to enhancing the scientific return of the Mars 2020 mission, since RDS measurements available in the PDS are lower than the corresponding incident solar fluxes at the surface because of this obscuration effect.

Dust accumulation shows a seasonal variability, with most of the net dust accumulation associated with the occurrence of regional dust storms leading to peaks in opacity. Skycam, which is not closely surrounded by magnets that may affect both dust deposition and removal, shows a very similar pattern, with minor quantitative differences.

After one MY, accumulated dust attenuates the incoming radiation by 25%–30%. This reduction is significantly smaller than previous estimates from InSight of 0.2%/sol. We have quantified dust deposition and removal rates at Jezero crater and western Elysium Planitia: while dust deposition rates are similar, the relative efficiency of dust removal mechanisms is nearly 10 times larger at Jezero.

We have modeled dust deposition based on measured dust opacities and on PCM-simulated dust deposition rates. While both models have a good performance in the long-term (semiannual or longer) evolution of the DCF, simulated dust deposition rates offer a better fit to the seasonal variability, supporting the hypothesis that considering multisize particle deposition can further improve the prediction capabilities of the model.

Projections of dust accumulation indicate that, as opposed to the InSight location, surfaces at Jezero crater are exposed to a significant net dust removal starting in the second MY of the mission. These results are encouraging for future missions operating in Jezero and similarly active dust lifting regions.

Data Availability Statement

MEDA measurements (Rodriguez-Manfredi and Torre Juarez, 2021) are stored in the NASA Planetary Data System (PDS) Atmospheres node (https://atmos.nmsu.edu/data_and_services/atmospheres_data/PERSEVERANCE/meda.html).

Acknowledgments
This research has been funded by the Spanish Ministry of Science and Innovation (MCIN)/State Agency of Research (AEI) project PID2021-126719OB-C41, funded by MCIN/AEI/10.13039/501100011033/FEDER, UE. GM wants to acknowledge JPL funding from USRA Contract Number 1638782. RL was supported via NASA InSight Participating Scientist Grant 80NSSC18K1626 and Perseverance/Supercam Contract #1655893 with the Jet Propulsion Laboratory. RH was supported by Grant PID2019-109467GB-I00 funded by MCIN/AEI/10.13039/501100011033 and by Grupos Gobierno Vasco IT1742-22.

References

Apestigue, V., Gonzalo, A., Jiménez, J. J., Boland, J., Lemmon, M., de Mingo, J. R., et al. (2022). Radiation and dust sensor for Mars environmental dynamic analyzer onboard M2020 rover. *Sensors*, *22*(8), 2907. https://doi.org/10.3390/s22082907

Bell, J. F., Maki, J. N., Mehall, G. L., Ravine, M. A., Caplinger, M. A., Bailey, Z. J., et al. (2021). The Mars 2020 Perseverance rover mast camera zoom (Mastcam-Z) multispectral, stereoscopic imaging investigation. *Space Science Reviews*, *217*(1), 1–40. https://doi.org/10.1007/s11214-020-00755-x

Crisp, D., Pathare, A., & Ewell, R. C. (2004). The performance of gallium arsenide/germanium solar cells at the Martian surface. *Acta Astronautica*, *54*(2), 83–101. https://doi.org/10.1016/s0094-5765(02)00287-4

Farley, K. A., Williford, K. H., Stack, K. M., Bhartia, R., Chen, A., de la Torre, M., et al. (2020). Mars 2020 mission overview. *Space Science Reviews*, *216*(8), 1–41. https://doi.org/10.1007/s11214-020-00762-y

Golombek, M., Hudson, T., Bailey, P., Balabanska, N., Marteau, E., Charalambous, C., et al. (2023). Results from InSight robotic arm activities. *Space Science Reviews*, *219*(3), 20. https://doi.org/10.1007/s11214-023-00964-0

Hueso, R., Newman, C. E., del Río-Gaztelurrutia, T., Munguira, A., Sánchez-Lavega, A., Toledo, D., et al. (2023). Convective vortices and dust devils detected and characterized by Mars 2020. *Journal of Geophysical Research: Planets*, *128*(2), e2022JE007516. https://doi.org/10.1029/2022je007516

Kass, D. M., Kleinböhl, A., McCleese, D. J., Schofield, J. T., & Smith, M. D. (2016). Interannual similarity in the Martian atmosphere during the dust storm season. *Geophysical Research Letters*, *43*(12), 6111–6118. https://doi.org/10.1002/2016GL068978

Kinch, K. M., Sohl-Dickstein, J., Bell III, J. F., Johnson, J. R., Goetz, W., & Landis, G. A. (2007). Dust deposition on the Mars exploration rover panoramic camera (Pancam) calibration targets. *Journal of Geophysical Research*, *112*(E6), E06S03. https://doi.org/10.1029/2006JE002807

Lemmon, M. T., Guzewich, S. D., Battalio, J. M., Malin, M. C., Vicente-Retortillo, A., Zorzano, M.-P., et al. (2024). The Mars Science Laboratory record of optical depth measurements via solar imaging. *Icarus*, *408*, 115821. https://doi.org/10.1016/j.icarus.2023.115821

Lemmon, M. T., Smith, M. D., Viudez-Moreiras, D., de la Torre-Juarez, M., Vicente-Retortillo, A., Munguira, A., et al. (2022). Dust, sand, and winds within an active Martian storm in Jezero crater. *Geophysical Research Letters*, *49*(17), e2022GL100126. https://doi.org/10.1029/2022gl100126

Lemmon, M. T., Wolff, M. J., Bell III, J. F., Smith, M. D., Cantor, B. A., & Smith, P. H. (2015). Dust aerosol, clouds, and the atmospheric optical depth record over 5 Mars years of the Mars Exploration Rover mission. *Icarus*, *251*, 96–111. https://doi.org/10.1016/j.icarus.2014.03.029

Lorenz, R. D., Lemmon, M. T., Maki, J., Banfield, D., Spiga, A., Charalambous, C., et al. (2020). Scientific observations with the InSight solar arrays: Dust, clouds, and eclipses on Mars. *Earth and Space Science*, *7*(5), e2019EA000992. https://doi.org/10.1029/2019ea000992

Lorenz, R. D., Martínez, G. M., Spiga, A., Vicente-Retortillo, A., Newman, C. E., Murdoch, N., et al. (2021). Lander and rover histories of dust accumulation on and removal from solar arrays on Mars. *Planetary and Space Science*, *207*, 105337. https://doi.org/10.1016/j.pss.2021.105337

Martínez, G. M., Newman, C. N., De Vicente-Retortillo, A., Fischer, E., Renno, N. O., Richardson, M. I., et al. (2017). The modern near-surface Martian climate: A review of in-situ meteorological data from Viking to Curiosity. *Space Science Reviews*, *212*(1–2), 295–338. https://doi.org/10.1007/s11214-017-0360-x

Martínez, G. M., Sebastián, E., Vicente-Retortillo, A., Smith, M. D., Johnson, J. R., Fischer, E., et al. (2023). Surface energy budget, albedo and thermal inertia at Jezero crater, Mars, as observed from the Mars 2020 MEDA instrument. *Journal of Geophysical Research: Planets*, *128*(2), e2022JE007537. https://doi.org/10.1029/2022je007537

Martín-Rubio, C., Vicente-Retortillo, A., Gómez, F., & Rodríguez-Manfredi, J. A. (2024). Interannual variability of regional dust storms between Mars years 24 and 36. *Icarus*, *412*, 115982. https://doi.org/10.1016/j.icarus.2024.115982

MEPAG. (2020). Mars scientific Goals, objectives, investigations, and priorities: 2020. In D. Banfield (Ed.), *White paper posted March, 2020 by the Mars Exploration Program Analysis Group (MEPAG)* (p. 89). Retrieved from https://mepag.jpl.nasa.gov/reports.cfm

MEPAG MCE-SAG Final Report. (2023). Mars Concurrent Exploration Science Analysis Group (MCE-SAG). In M. Mischna & B. Horgan (Eds.), *Posted on 18 July 2023 by the Mars exploration Program Analysis Group* (p. 94). Retrieved from https://www.lpi.usra.edu/mepag/reports/reports/MCE_SAG_Final_Report.pdf

National Academies of Sciences, Engineering, and Medicine. (2022). Origins, worlds, and life: A decadal strategy for planetary science and astrobiology 2023–2032.

Newman, C. E., Hueso, R., Lemmon, M. T., Munguira, A., Vicente-Retortillo, Á., Apestigue, V., et al. (2022). The dynamic atmospheric and aeolian environment of Jezero crater, Mars. *Science Advances*, *8*(21), eabn3783. https://doi.org/10.1126/sciadv.abn3783

Rodriguez-Manfredi, J. A., & de la Torre Juarez, M. (2021). Mars 2020 Perseverance Rover Mars Environmental Dynamics Analyzer (MEDA) experiment data record (EDR) and reduced data record (RDR) data products archive bundle. *NASA Planetary Data System Atmospheres Node*. https://doi.org/10.17189/1522849

Rodriguez-Manfredi, J. A., De la Torre Juárez, M., Alonso, A., Apéstigue, V., Arruego, I., Atienza, T., et al. (2021). The Mars Environmental Dynamics Analyzer (MEDA): A suite of environmental sensors for the Mars 2020 mission. *Space Science Reviews*, *217*(3), 1–86. https://doi.org/10.1007/s11214-021-00816-9

Rover Team. (1997). Characterization of the Martian surface deposits by the Mars pathfinder rover, sojourner. *Science*, *278*(5344), 1765–1768. https://doi.org/10.1126/science.278.5344.1765

Sebastián, E., Martínez, G., Ramos, M., Haenschke, F., Ferrándiz, R., Fernández, M., & Rodriguez-Manfredi, J.-A. (2020). Radiometric and angular calibration tests for the MEDA-TIRS radiometer onboard NASA′s Mars 2020 mission. *Measurement*, *164*, 107968. https://doi.org/10.1016/j.measurement.2020

Spiga, A., Murdoch, N., Lorenz, R., Forget, F., Newman, C., Rodriguez, S., et al. (2021). A study of daytime convective vortices and turbulence in the Martian planetary boundary layer based on half-a-year of InSight atmospheric measurements and large-eddy simulations. *Journal of Geophysical Research: Planets*, *126*(1), e2020JE006511. https://doi.org/10.1029/2020JE006511

Stella, P. M., & Herman, J. A. (2010). The Mars surface environment and solar array performance. In *Photovoltaic Specialists Conference (PVSC), 2010 35th IEEE* (pp. 002631–002635).

Toledo, D., Apéstigue, V., Arruego, I., Lemmon, M., Gómez, L., Montoro, A. D. F., et al. (2023). Dust devil frequency of occurrence and radiative effects at Jezero crater, Mars, as measured by MEDA Radiation and Dust Sensor (RDS). *Journal of Geophysical Research: Planets*, *128*(1), e2022JE007494. https://doi.org/10.1029/2022je007494

Vicente-Retortillo, A., Martínez, G. M., Lemmon, M. T., Hueso, R., Johnson, J. R., Sullivan, R., et al. (2023). Dust lifting through surface albedo changes at Jezero crater, Mars. *Journal of Geophysical Research: Planets*, *128*(4), e2022JE007672. https://doi.org/10.1029/2022JE007672

Vicente-Retortillo, Á., Martínez, G. M., Rennó, N., Newman, C. E., Ordonez-Etxeberria, I., Lemmon, M. T., et al. (2018). Seasonal deposition and lifting of dust on Mars as observed by the Curiosity rover. *Scientific Reports*, *8*(1), 17576. https://doi.org/10.1038/s41598-018-35946-8

Vicente-Retortillo, Á., Martínez, G. M., Renno, N. O., Lemmon, M. T., & de la Torre-Juárez, M. (2017). Determination of dust aerosol particle size at Gale Crater using REMS UVS and Mastcam measurements. *Geophysical Research Letters*, *44*(8), 3502–3508. https://doi.org/10.1002/2017GL072589

Vicente-Retortillo, A., Martínez, G. M., Rennó, N. O., Lemmon, M. T., de la Torre-Juárez, M., & Gómez-Elvira, J. (2020). In situ UV Measurements by MSL/REMS: Dust deposition and angular response corrections. *Space Science Reviews*, *216*(5), 97. https://doi.org/10.1007/s11214-020-00722-6

Vicente-Retortillo, Á., Valero, F., Vázquez, L., & Martínez, G. M. (2015). A model to calculate solar radiation fluxes on the Martian surface. *Journal of Space Weather and Space Climate*, *5*, A33. https://doi.org/10.1051/swsc/2015035

Wolff, M. J., Clancy, R. T., Goguen, J. D., Malin, M. C., & Cantor, B. A. (2010). Ultraviolet dust aerosol properties as observed by MARCI. *Icarus*, *208*(1), 143–155. https://doi.org/10.1016/j.icarus.2010.01.010

Wolff, M. J., Smith, M. D., Clancy, R. T., Arvidson, R., Kahre, M., Seelos, F., et al. (2009). Wavelength dependence of dust aerosol single scattering albedo as observed by the Compact Reconnaissance Imaging Spectrometer. *Journal of Geophysical Research*, *114*(E2), E00D04. https://doi.org/10.1029/2009je003350

Yingst, R. A., Bray, S., Herkenhoff, K., Lemmon, M., Minitti, M. E., Schmidt, M., et al. (2020). Dust cover on Curiosity′s Mars Hand Lens Imager (MAHLI) calibration target: Implications for deposition and removal mechanisms. *Icarus*, *351*, 113872. https://doi.org/10.1016/j.icarus.2020.113872

References From the Supporting Information

Forget, F., Hourdin, F., Fournier, R., Hourdin, C., Talagrand, O., Collins, M., et al. (1999). Improved general circulation models of the Martian atmosphere from the surface to above 80 km. *Journal of Geophysical Research*, *104*(E10), 24155–24175. https://doi.org/10.1029/1999je001025

Madeleine, J.-B., Forget, F., Millour, E., Montabone, L., & Wolff, M. J. (2011). Revisiting the radiative impact of dust on Mars using the LMD global climate model. *Journal of Geophysical Research: Planets*, *116*(E11), E11010. https://doi.org/10.1029/2011JE003855

Montabone, L., Forget, F., Millour, E., Wilson, R. J., Lewis, S. R., Cantor, B., et al. (2015). Eight-year climatology of dust optical depth on Mars. *Icarus*, *251*, 65–95. https://doi.org/10.1016/j.icarus.2014.12.034

Navarro, T., Madeleine, J. B., Forget, F., Spiga, A., Millour, E., Montmessin, F., & Määttänen, A. (2014). Global climate modeling of the Martian water cycle with improved microphysics and radiatively active water ice clouds. *Journal of Geophysical Research: Planets*, *119*(7), 1479–1495. https://doi.org/10.1002/2013je004550

Rossow, W. B. (1978). Cloud microphysics: Analysis of the clouds of Earth, Venus, Mars and Jupiter. *Icarus*, *36*(1), 1–50. https://doi.org/10.1016/0019-1035(78)90072-6